Biosensors and Bioelectronics 285 (2025) 117529



Contents lists available at ScienceDirect

Biosensors and Bioelectronics

journal homepage: www.elsevier.com/locate/bios



One-pot RPA-CRISPR/Cas12a integrated dual-mode electrochemical lateral flow strip for ultrasensitive and precise detection of *Salmonella*

Qi Chen [a,1], Hang Wang [a,1], Haoyang Xu [a], Yubo Peng [a], Bangben Yao [b], Zhaoran Chen [b], Jiening Yang [c], Samuel Adeloju [d,*], Wei Chen [a,**]

[a] Engineering Research Center of Bio-process, MOE, School of Food and Biological Engineering, Intelligent Manufacturing Institute, Hefei University of Technology, Hefei, 230009, PR China
[b] Anhui Province Institute of Product Quality Supervision & Inspection, Hefei, 230051, PR China
[c] Technical Centre for Animal, Plant and Food Inspection and Quarantine of Shanghai Customs, Shanghai, 200135, PR China
[d] School of Chemistry, Monash University, Clayton, Victoria, 3800, Australia

ARTICLE INFO

Keywords:
One-pot
Electrochemical
Lateral flow strip
OPRCC-eLFS
Ultrasensitive
Salmonella
Dual-mode biosensing platform

ABSTRACT

Rapid and accurate screening of pathogenic contamination is essential for timely intervention and infection prevention. In this work, one-pot RPA-CRISPR/Cas12a strategy combined with an innovative electrochemical lateral flow strip (OPRCC-eLFS) was presented for ultrasensitive and precise detection of *Salmonella*. Highly sensitive dual-mode detection of *Salmonella* in various samples has been simultaneously achieved with electrochemical detection limit of 3.84 CFU/mL and visual detection limit of 384 CFU/mL, respectively, with improved detection efficiency and prevention of uncapping-related aerosol-contamination. This dual-mode biosensing platform demonstrates exceptional stability, remarkable sensitivity, and robust on-site quantification capability, emphasizing its potential in food safety monitoring and disease prevention.

1. Introduction

A major global public health risk to consumers is food contamination by bacterial infections (Li et al., 2023; Vieira et al., 2022; Wei and Zhao, 2021). Annually, microbial contamination results in over 600 million cases of foodborne illness and approximately 420,000 deaths worldwide (Gao et al., 2022; Lee and Yoon, 2021; Ma et al., 2023). *Salmonella* has emerged as one of the most prevalent causes of foodborne disease due to its remarkable environmental tolerance and rapid growth rate (Shen et al., 2022). Typically, infection occurs through the consumption of untreated water and contaminated food, leading to symptoms of abdominal cramps, fever, diarrhea, and even death. Bacterial infection therefore poses serious public health risks and can result in substantial economic losses (Galán, 2021; Shen et al., 2021). Consequently, regulatory agencies worldwide have established strict allowable limits for *Salmonella* residues in various food samples (Jiang et al., 2024).

Numerous methods have been developed for *Salmonella* detection, including traditional culture-assisted plate counting (Qiu et al., 2023), polymerase chain reaction (PCR) (Fu et al., 2021; Shen et al., 2021), quantitative real-time PCR (qPCR) (Liu et al., 2018), and antigen-based immune-recognition assay (Gu et al., 2022; Ren et al., 2022). However, most of these current existing detection methods are often time-consuming or require expensive equipment, and are usually conducted in professional centered laboratories by trained personnel (Younes et al., 2024).

Consequently, there has been a growing need for methods that are simple to operate, of high sensitivity and accuracy that are effective in supporting routine food safety monitoring.

Due to its high specificity and the programmability of CRISPR, it has been extensively adopted across various fields for precise recognition and signal amplification (Cheng et al., 2022; Wu et al., 2024). While CRISPR-based protocols demonstrate powerful and robust signal amplification capabilities, the sensitivity is still inadequate for direct analysis of samples without nucleic acid amplification (Zhang et al., 2024). To further improve the sensitivity, CRISPR is usually utilized and combined with nucleic acid amplification methods (Hu et al., 2023; Song et al., 2022; Wang et al., 2024; Yin et al., 2024). Among these, recombinase polymerase amplification (RPA) has emerged as one of the

* Corresponding author.
** Corresponding author.
E-mail addresses: sam.adeloju@monash.edu (S. Adeloju), chenweishnu@163.com (W. Chen).
[1] These two authors contributed equally to this research.

https://doi.org/10.1016/j.bios.2025.117529
Received 12 February 2025; Received in revised form 10 April 2025; Accepted 29 April 2025
Available online 1 May 2025
0956-5663/© 2025 Elsevier B.V. All rights are reserved, including those for text and data mining, AI training, and similar technologies.

most widely utilized approaches in conjunction with CRISPR, owing to its simplicity, shorter reaction time, and unique isothermal condition (Ahamed et al., 2024; Yang et al., 2024). Currently, among common Cas families, application of Cas9 needs the complicated design of tracrRNA-crRNA with just proved lower *trans*-cleavage effect (Chen et al., 2024) while the Cas13 with the *trans*-cleavage effect to single-stranded RNA probe, which can induce the false results due to the degradation of RNA probe. As one of the most mature and widely adopted subtype of Cas12, the Cas12a holds the superior random *trans*-cleavage effect to the single-stranded DNA probe and has been widely utilized. However, most of RPA-CRISPR/Cas12a-mediated methods strictly require separated operational steps to avoid the non-specific cleavage of RPA raw reagents. Traditional two-step operations not only increase complexity but also elevates the risk of aerosol contaminations due to tube opening, thereby limiting their widespread applications (Mao et al., 2023; Zhong et al., 2025). Ideally, integrating isothermal amplification with CRISPR/Cas12a in the single-tube format is essential. However, this integration poses significant and critical challenges, as the *trans*-cleavage activity of the Cas12a protein can non-specifically cleave newly synthesized amplicons or unreacted primers, resulting in a remarkable reduction in amplification efficiency.

Various strategies have been explored to address this issue, including optically activating crRNA post-amplification (Shen et al., 2022), utilizing glycerol and paraffin for the physical separation of two reaction systems (Lin et al., 2022; Tan et al., 2024), employing suboptimal PAMs to mitigate CRISPR *trans*-cleavage (Wang et al., 2023), and implementing asymmetric RPA amplification (Yang et al., 2024). However, these approaches still present certain limitations including non-real one-pot, or compromised amplification efficiency. To overcome these challenges, we designed efficient primers to enhance the RPA and meticulously optimized the key components of both RPA and CRISPR/Cas12a systems. This optimization enabled us to achieve a balanced reaction system, resulting in a truly integrated one-pot reaction with significantly improved simplicity and sensitivity.

The reliability of the analytical modes is crucial for expanding their applications. Lateral flow strips (LFS) have emerged as prominent and successful diagnostic tools due to their simplicity, cost-effectiveness, stability, and rapid judgements (Younes et al., 2024). Currently, LFSs are utilized extensively in food safety, environmental monitoring, and disease diagnosis, owing to their quick response and user-friendly design (Wang et al., 2022). However, while conventional LFSs are straightforward and economical, they exhibit limitations in sensitivity and quantification ability, yielding only the colorimetric signal-assisted qualitative results (Li et al., 2024). To overcome these intrinsic limitations, integrating LFS with more sensitive electrochemical techniques is essential for developing an effective dual-mode detection strategy. Compared to single-mode techniques, the dual-mode approach combines two complementary detection modes, enabling simultaneous qualitative screening and quantitative analysis. This integration enhances sensitivity, broadens applicability, and improves accuracy. Moreover, dual-mode analysis mitigates the inherent limitations of single-mode sensing methods by leveraging the unique advantages of each mode, creating a synergistic effect that greatly enhances analytical performance.

In response to the highlighted issues, we have developed a streamlined one-pot RPA-CRISPR/Cas12a integrated electrochemical lateral flow strip (**OPRCC-eLFS**) for accurate detection of target *Salmonella*. This innovative approach enables rapid, semi-quantitative, and quantitative detection of *Salmonella* across in various applications. In this newly designed approach, we utilized gold nanoparticles (AuNPs) simultaneously as a colorimetric signal molecule and as a catalytic tag for *in-situ* redox reactions. The redox response involves the reduction of ferricyanide ($[Fe(CN)_6]^{3-}$, Fe^{3+}) to Fe^{2+} by ammonia-borane (H_3N-BH_3, AB) as the reductant in the presence of AuNPs, resulting in a significant increase in current output and thereby enhancing the sensitivity of eLFS. This dual-mode sensing system presents several advantages, which renders it a robust tool for rapid and reliable pathogen detection.

2. Experimental section

2.1. Chemicals and apparatus

Streptavidin (SAV), DNA probes (refer to Table S1), 20 × PBS (pH 7.4–7.6), 1 M Tris-HCl (pH 7.4 and pH 8.0), and bovine serum albumin (BSA) were acquired from Sangon Biotech (Shanghai, China). Tween-20, potassium ferricyanide ($K_3[Fe(CN)_6]$), ammonia borane ($NH_3{\cdot}BH_3$), trisodium citrate ($C_6H_5Na_3O_7$), sodium borohydride ($NaBH_4$), hydroxylamine hydrochloride ($NH_2OH{\cdot}HCl$), ascorbic acid (AA), and other common reagents were sourced from Sinopharm Chemical Reagent (Shanghai, China). Chloroauric acid tetrahydrate ($HAuCl_4$) was obtained from J&K Scientific (Beijing, China), while RPA kits were supplied by GenDx Biotech (Suzhou, China). The bacterial genomic DNA extraction kit was provided by Tiangen Biotech (Beijing, China). NEBuffer1 and EnGen® Lba Cas12a were procured from New England Biolabs Inc., and crRNA (refer to Table S1) was purchased from Bilig Biotech (Shanghai, China). The nitrocellulose membrane (AE99) was sourced from Wen Xinjie Biotech (Shanghai, China). The anti-FITC antibody was purchased from Abgree Bio (Guangzhou, China). The screen-printed carbon electrode (SPCE) was provided by Shenzhen Refresh Biosensing Technology., LTD (Shenzhen, China). The universal dye-based fluorescent quantitative PCR kit for *Salmonella* (Cat. No. YB1279L) was ordered from Shanghai Yubo Biotechnology Co., Ltd.

All electrochemical measurements were performed at room temperature using a CHI 660D Electrochemical Workstation from Shanghai Chenhua Instrument Co., Ltd. The catalytic reduction of the Fe^{3+}/AuNP/AB system was analyzed using a microplate reader (MK3) from Thermo Fisher Scientific (USA). The Fluorescent spectra were measured using a F97 Pro fluorescence spectrophotometer (Shanghai Cold 116 Light Technology Co., Ltd.).

2.2. Development of one-pot RPA-CRISPR/Cas12a (OPRCC) assay

The one-pot RPA-CRISPR/Cas12a system was initially set as 25 μL containing pre-freeze-dried powder, 0.6 μM forward and reverse primers, 1 × NEBuffer1, 0.02 μM Cas12a, 0.1 μM crRNA, 0.6 μM FAM-ssDNA-BHQ, and 10 mM magnesium acetate. DEPC-treated water was used in this system. The initial fluorescence detection conditions were set at 37 °C for 60 min. After optimization, the forward and reverse primer concentrations were increased to 1.2 μM, while the crRNA and Cas12a concentrations were adjusted to 0.16 μM and 0.04 μM, respectively. The reaction temperature and duration were optimized to 41 °C and 90 min, respectively.

2.3. Construction of eLFS

The eLFS was designed and constructed in the similar way as the traditional LFS reported in our previous research (Li et al., 2023), with the key distinction of being incorporated with SPCE positioned between the nitrocellulose (NC) membrane and the backing pad of LFS. Briefly, 1000 μL of AuNPs were adjusted to the desired pH using 10 μL 0.1 M potassium carbonate (K_2CO_3). Subsequently, anti-FITC antibody conjugates were prepared by coupling 4 μg of the anti-FITC antibody to the surface of the AuNPs, which were then deposited onto the conjugate pads. For the spraying process, 1 mg/mL of streptavidin (SAV) and goat anti-mouse antibody were coated onto the NC membrane to establish the test (T) line and control (C) line, respectively. The components, including the sample pad, conjugate pad, SPCE, NC membrane, and absorbent pad were assembled sequentially onto the backing pad. The SPCE was strategically inserted between the backing pad and the NC membrane, ensuring that its working electrode was closely aligned with the T line on the NC membrane. Details of the assembly process are provided in Fig. S1.

2.4. Detection of Salmonella with the developed OPRCC-eLFS

For OPRCC, this one-pot RPA-CRISPR/Cas12a system was developed with the volume of 25 μL containing pre-freeze-dried powder, 1.2 μM forward and reverse primers, 1 × NEBuffer1, 0.04 μM Cas12a, 0.16 μM crRNA, 10 nM FITC-ssDNA-Bio, and 10 mM magnesium acetate. DEPC-treated water was used in the reaction system. The reaction was carried out at 41 °C for 90 min. For eLFS, 1.5 μL of the one-pot reaction product was mixed with 48.5 μL running solution (10 mM Tris-HCl, 2 × SSC, 5 mM KCl, 5 mM $MgCl_2$, 0.5 % PEG, 20000, 1 mM CTAB, 1 % Tween-20, 1 % BSA, pH 8.0) and dropped onto the sample pad for visual analysis. After 10 min, 100 μL of the catalytic solution (containing 5 mM $K_3[Fe(CN)_6]$, 5 mM AB, and 1 × PBS, pH 7.4) was added to the T line of eLFS. The electrochemical signal was measured after 2 min.

2.5. Real sample preparation and DNA extraction

The standard *Salmonella* strain (ATCC 14028) was sourced from the Anhui Province Institute of Product Quality Supervision & Inspection at an initial concentration of 3.84 × 10^7 CFU/mL. Milk, orange juice, and egg samples used for practical testing were purchased from a local supermarket and verified to be free of *Salmonella* contamination through culture-based methods. To assess the reliability and accuracy of the methodology, simulated *Salmonella*-contaminated samples were prepared. Typically, 1 mL of the 3.84 × 10^7 CFU/mL bacterial solution was centrifuged at 10,000 g for 10 min, and the pellet was resuspended in 1 mL of milk, orange juice, or egg samples. The spiked samples were then serially diluted in their respective food matrices to generate *Salmonella* samples with varying concentrations. DNA was extracted following the TIANamp Bacteria DNA Extraction Kit instructions and resuspended in 50 μL of 1 × TE buffer.

2.6. Fluorescent and electrochemical signal measurement

Fluorescence intensity measurement: Set the excitation wavelength at 490 nm and record the emission spectrum from 500 to 650 nm. Set both excitation and emission slit widths of 10 nm, and maintain the photomultiplier tube (PMT) voltage at 650 V.

Electrochemical measurement: Set the scan rate of cyclic voltammetry (CV) of 50 mV/s. For chronoamperometric detection, apply a constant voltage of 0.3 V for 50 s and monitor the terminal current after the stabilization of redox reaction (Fe^{3+}/AuNPs/AB).

3. Results and discussion

3.1. Design principle of OPRCC-eLFS

The overall principles of the proposed OPRCC-eLFS for *Salmonella* detection are depicted in details in Fig. 1. As shown in Fig. 1A. As the first step, the one-pot reaction system based on RPA-CRISPR/Cas12a is developed. By designing efficient primers and optimizing reaction conditions for both RPA and CRISPR/Cas12a, respectively, the system is able to achieve an optimal balance between these two reactions. The balance means that the RPA can produce enormous amplicons to activate the *trans*-cleavage effect of Cas12a while the activated CRISPR-Cas12a will not consume the essential reagents and decrease the efficiency of RPA. Fig. 1B illustrates the practical workflow for detecting RPA-CRISPR/Cas12a reaction products with eLFS. Unlike conventional LFS, the eLFS includes an additional assembly of SPCE between the NC membrane and the backing pad. The SPCE's working electrode is precisely aligned with the T line on the NC membrane. In the detection process, a catalytic redox step, which is absent in traditional LFS, will be completed within just 2 min. Typically, Fe^{3+}, AB, and AuNPs serve as the mediator, reducing agent, and catalytic tag, respectively. This reaction occurs exclusively in the presence of AuNPs, which catalyze the

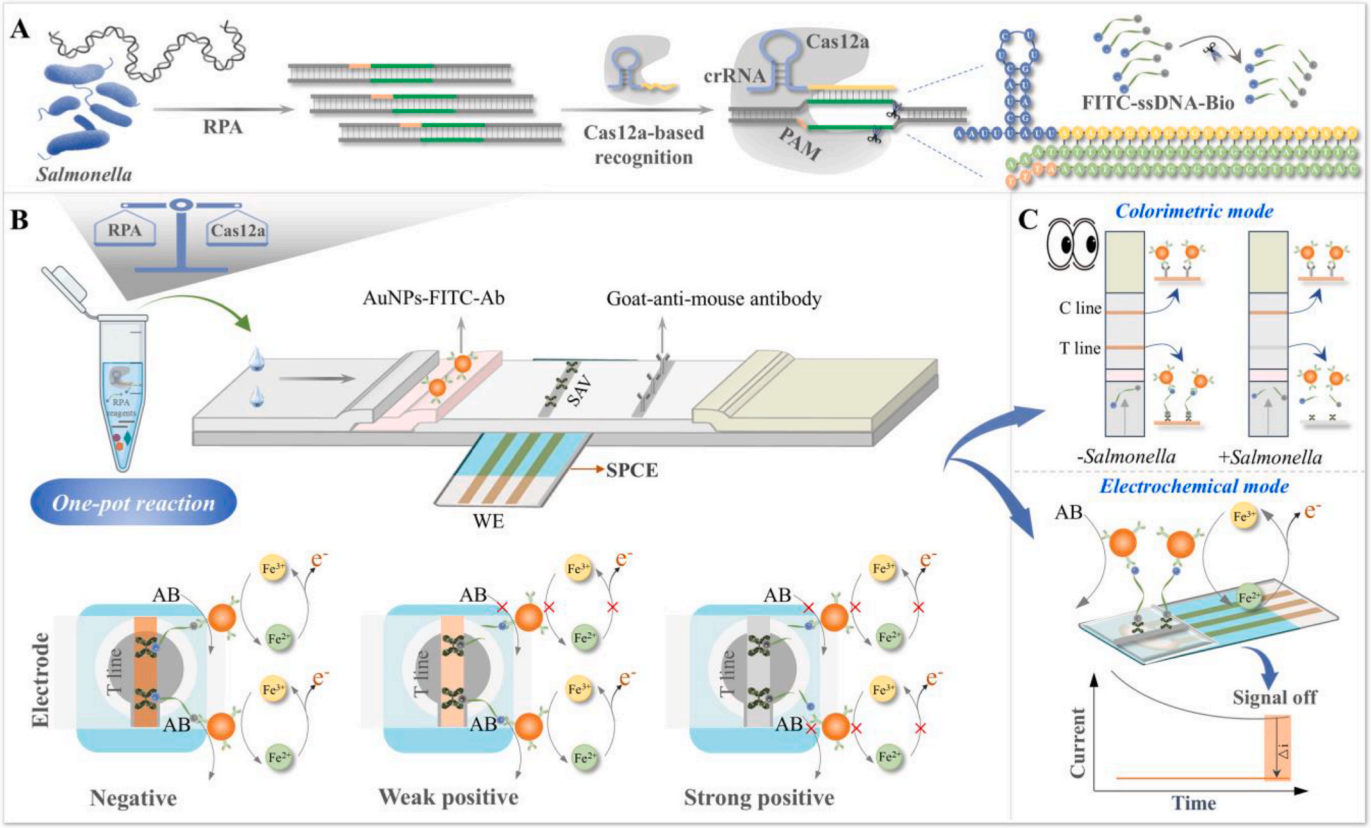


Fig. 1. Schematic illustration of the OPRCC-eLFS for accurate quantification of *Salmonella*.

reduction of Fe^{3+} to Fe^{2+} by AB.

For the detection and signal output mechanism with above eLFS, in the absence of target *Salmonella*, RPA will not be processed and no double-stranded amplicons will be produced, which will not activate the *trans*-cleavage of Cas12a. Then, the intact signal probe can be captured on the T line by the specific recognition between the biotin on the probe and the pre-immobilized streptavidin (SAV) on the T line. Meanwhile, the AuNPs-Ab $_{FITC}$ complex could also be retained on the T line by the specific recognition between FITC on the probe and the Ab on the AuNPs. This simultaneous recognition of FITC and biotin on the probe will cause the retention of AuNPs on T line and the coloration of T line for colorimetric signal output. However, for the target gene analysis, in the presence of target *Salmonella*, RPA generates enormous double-stranded DNA, which can be specifically recognized by crRNA, activating Cas12a′s *trans*-cleavage activity. This activation cleaves the Bio-ssDNA-FITC signal probe. And for this cleaved signal probe only the biotin-modified segments could be captured onto the T line while the FITC-modified segments of the probe recognized by the AuNPs-Ab $_{FITC}$ complex will not be retained onto the T line and no or weak coloration of T line will occur. Additionally, when the catalytic solution is applied onto the T line, the lack of captured catalytic tag (AuNPs) significantly reduces redox reaction efficiency, preventing Fe^{3+} reduction to Fe^{2+} by AB, resulting in a low current response in the electrochemical quantitative detection mode. Besides, considering the future on-site screening applications, the chronoamperometric method is adopted for measurement and signal output due to the simple parameter setting and operation by non-professional personnel. Notably, the goat anti-mouse antibody pre-modified on the C line captures AuNPs-FITC-Ab regardless of the presence of *Salmonella* or not, ensuring a consistent color signal on the C line. In summary, for negative samples, both the C and T lines are visible on the eLFS, and electrochemical detection yields a high current response. On the other hand, for positive samples, only the C line is visible (or the T line appears faint), and the current response is low (Fig. 1C). Meanwhile, the common non-specific amplification in RPA could be well avoided with the designed CRISPR/Cas12a to guarantee the specificity of the designed OPRCC-eLFS. Thus, enabling the *in-situ* electrochemical measurement on LFS to output the quantitative results directly with excellent sensitivity for efficient and accurate quantitative detection of *Salmonella*.

3.2. Mechanistic investigations of redox processes

To construct the eLFS for quantitative measurement, the establishment of catalytic AuNPs-depended redox reaction system is a critical step. The fundamental strategy for selecting stable redox components for the system is as follows: (i) Fe^{3+} can be rapidly and efficiently reduced catalytically in the presence of both AuNP and AB; (ii) the electron mediator ($Fe^{2+}/^{3+}$) exhibits remarkable self-stability; and (iii) (iV) the direct reduction of Fe^{3+} by either AB or AuNP alone is slow or nearly nonexistent (Fig. 2A). The redox system with Fe^{3+}, AB, and AuNPs acting as the mediator, reductant, and catalytic tag, respectively, was carefully validated. The results in Fig. 2B show that only under the condition of co-existence of the three components (Fe^{3+} +AB + AuNPs and AuNPs + Fe^{3+} + AB), the redox reaction could occur to result in the exhaustion of Fe^{3+}, leading to the disappearance of the characteristic peaks of Fe^{3+} at 420 nm and the decreased and red-shift of typical peak of AuNPs at 520 nm, respectively. The red-shift of the typical peak of AuNPs to the higher wavelength indicates the aggregation of AuNPs in the catalytic redox system, which may be attributed to the variation of the electric charges of the solution. For all other comparison control groups in Fig. 2B, the characteristic peak signal of Fe^{3+} remains the same, thus indicating an exclusive condition for the reduction of Fe^{3+} to Fe^{2+} by AB in the presence of AuNPs for electrochemical measurements.

Furthermore, the feasibility of the designed strategy was verified by

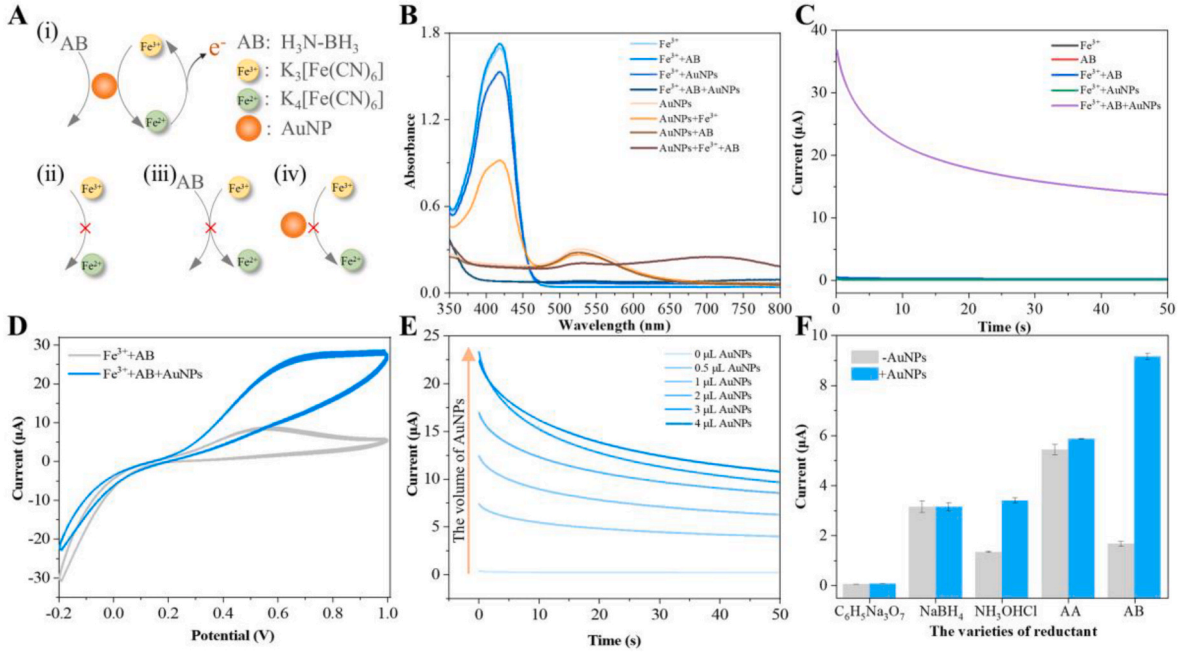


Fig. 2. Feasibility demonstration of the Fe^{3+}/AuNPs/AB redox system. (A) Schematic representation of the catalytic reduction of Fe^{3+}/AuNPs/AB. (B) UV/vis absorption spectra for the catalytic reduction of Fe^{3+} by AB with the AuNPs. The blue curve series represents a reaction that 6 μL of a 10 × concentrated AuNPs was added into the Fe^{3+} and AB with the concentration of 50 mM (total 200 μL). In the absence of AuNPs, an equivalent volume (6 μL) of ultrapure water was added; The brown curve series corresponds to a reaction that 10 μL 50 mM Fe^{3+} and AB were added separately or together into the AuNPs solution (total 200 μL). (C) The chronoamperometric response of Fe^{3+} and AB was recorded at +0.3 V, with or without AuNPs. Fe^{3+} and AB were both prepared at a concentration of 5.0 mM in 10 mM PBS, with the AuNP concentration identical to that in condition (B). (D) Cyclic voltammetry (CV) analyses of Fe^{3+} and AB were performed in the absence and presence of AuNPs, maintaining the same concentrations as in condition (C). Each experiment was performed in five parallels measurements to ensure reproducibility. (E) Influence of AuNP concentration on the activity of the Fe^{3+}/AuNPs/AB redox system. (F) Impact of different reducing agents on the activity of the redox system. (For interpretation of the references to color in this figure legend, the reader is referred to the Web version of this article.)

other electrochemical modes of detection. Both the i-t and cyclic voltammetry in Fig. 2C and D clearly demonstrate the similar outcomes for the electrochemical measurements. Of great significance for quantitative electrochemical measurement on T line of the eLFS, the effect of the amount of AuNPs on the sensing current was also considered. A positive dependence relationship is observed as shown in Fig. 2E, which strongly support the feasibility of quantitative analysis conducted on the T line of eLFS. Besides, to achieve the best redox efficiency for quantitative analysis, various reducing agents were tested and AB was considered as the most stable and exhibited robust reducing performance in the presence of AuNPs (Fig. 2F).

3.3. Feasibility verification and parameter optimization of OPRCC-eLFS

The feasibility of the one-pot RPA-CRISPR/Cas12a system for detecting *Salmonella* was demonstrated by integrating two primary units: RPA for target DNA amplification and Cas12a for sequence-specific recognition.

Initially, the performances of RPA and CRISPR/Cas12a in the one-pot reaction were evaluated, and the procedural details are provided in Fig. 3A. As expected, the results in Fig. 3B indicate that in the designed one-pot RPA-CRISPR/Cas12a system, the presence of target DNA extracted from *Salmonella* (3.84×10^6 CFU/mL) could induce a substantial increase in fluorescent output signals compared to other groups lacking the essential components for amplification or cleavage. This significant difference in fluorescence signals clearly demonstrates the ability to successful utilize this one-pot RPA-CRISPR/Cas12a strategy for detection of *Salmonella*.

Subsequently, the dual-labeled Bio-ssDNA-FITC probe was adopted for the verification of OPRCC-eLFS (see details in Fig. 3C). In the presence of target *Salmonella*, the isothermal produced amplicons activate the cleavage property of Cas12a and the dual-labeled Bio-ssDNA-FITC probes were hydrolyzed into pieces. Then, less dual-labeled Bio-ssDNA-FITC probes are captured on the T line of eLFS and the corresponding colorimetric signal on T line was decreased while other groups did not induce the T line signal variations compared to the negative control (Fig. 3D). Notably, the T line in Fig. 3D was further treated with the catalytic solution, then the current responses were measured *in situ* as shown in the scheme (Fig. 1). Similar results were obtained with the obvious decrease of sensing current on the T line of the positive group while not for others (Fig. 3E). The corresponding quantitative histogram in Fig. 3F also corroborate the high feasibility of this proposed OPRCC-eLFS method.

As designed, to achieve a highly sensitive, rapid, convenient and quantitative detection, the one-pot RPA-CRISPR/Cas12a system was innovatively integrated with the electrochemical lateral flow strip, as OPRCC-eLFS, with a multi-mode detection by LFS and an electrochemical sensor. Several critical parameters were optimized to obtain a rationally balanced amplification and Cas12a cleavage system. Magnesium acetate is a crucial activator of the RPA reaction, directly influencing DNA amplification efficiency. Similarly, primer concentration affects the amplification rate. Insufficient primer concentrations result in weak signal output, whereas excessive concentrations may interfere with Cas12a trans-cleavage activity, reducing detection efficiency. Through optimization, the optimal magnesium acetate concentration and primer concentration were determined to be 10 mM and 1.2 μM, respectively, yielding improved sensing performance. The concentrations of crRNA and Cas12a directly impact Cas12a trans-cleavage activity. While higher concentrations can enhance cleavage efficiency, excessive levels may degrade unreacted primers too quickly, compromising RPA amplification and reducing overall signal strength. Optimization experiments revealed that the strongest fluorescence signal and the highest signal-to-noise ratio were achieved with 0.16 μM crRNA and 0.04 μM Cas12a. The reaction time and temperature of the one-pot system play a critical role in RPA amplification efficiency and Cas12a trans-cleavage activity. Optimization studies demonstrated that a reaction time of 90 min at 41 °C produced the highest detection signal (See details in Fig. S2). And under the optimized conditions, this proposed one-pot RPA-CRISPR/Cas12a produced a comparable fluorescence signal to that of the traditional two-step RPA and CRISPR/Cas protocol (Fig. S3). Besides, the concentration of dual-labeled Bio-ssDNA-FITC probe and the loading volume of the one-pot amplification product were

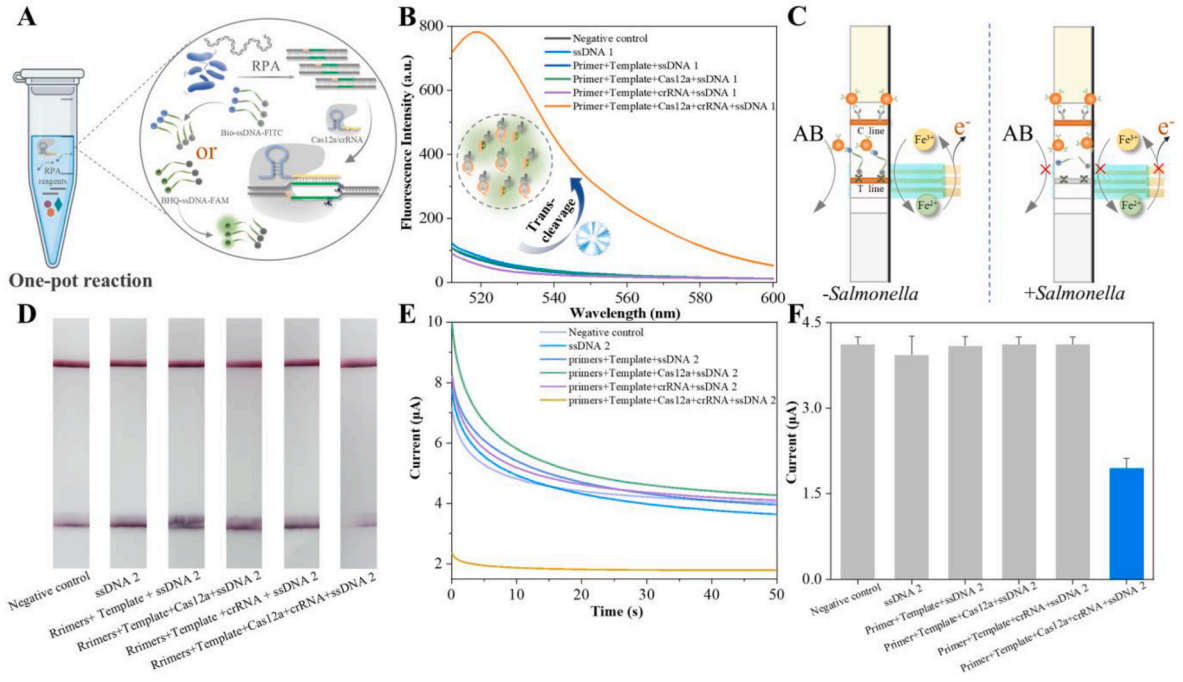


Fig. 3. The feasibility of the OPRCC-eLFS method was evaluated through comprehensive analyses. (A) Schematic of one-pot RPA-CRISPR/Cas12a reaction mechanism. (B) Fluorescence assay validate the efficiency of the one-pot RPA-CRISPR/Cas12a method. (C) Schematic illustration of the eLFS for detecting *Salmonella*. (D) Visual validation demonstrates the detection capability of the OPRCC-eLFS method. (E) Electrochemical analysis further confirms the method's effectiveness. (F) The current signal intensity corresponding to the electrochemical conditions in (E) is presented.

considered for OPRCC-eLFS measurement and 10 nM of the probe concentration (Fig. S4A) and 1.5 μL of the loading volume of amplicons (Fig. S4B) gave the best colorimetric and electrochemical signals.

3.4. Sensing performance of OPRCC-eLFS for Salmonella detection

Under the optimized sensing conditions, comprehensive sensing performance studies of OPRCC-eLFS were carried out for detecting *Salmonella*. Firstly, the rapid colorimetric qualitative screening of *Salmonella* was performed in three parallel eLFS tests as shown in Fig. 4A. Evidently, the colorimetric optical signal on the T line decreased with increasing *Salmonella* concentration from 3.84 to 3.84 × 10^7 CFU/mL. Even though, the routine gray intensity treatment of the T line on LFS was also conducted for obtaining quantitative analysis information. Results in Fig. S5 demonstrated the quantitative treated results of the gray intensities on T line of eLFS. Meanwhile, to get the more accurate results, the quantitative electrochemical measurement was further performed by adding a catalytic solution onto the T line of eLFS and the *in-situ* chronoamperometric data were recoded and presented in Fig. 4B. The linear relationship obtained from the electrochemical signals on the T line of eLFS is shown in Fig. 4C with equation Y = 3.423–0.464 X (R^2 = 0.985, Y, the current value on T line; X, the logarithm of *Salmonella* concentration). The visual detection limit of the OPRCC-eLFS was 38.4 CFU/mL, while the electrochemical detection limit was calculated to be as low as 1.96 CFU/mL using the 3σ/k criterion, where σ represents the standard deviation of the blank and k is the slope of the calibration curve. Compared to any single-mode detection, the OPRCC-eLFS dual-mode strategy realized the simultaneous qualitative screening and quantitative determination. The sensitivity of the single LFS mode was improved by the OPRCC-eLFS dual-mode strategy while the accuracy could be guaranteed by the mutual calibration of two modes, minimizing the false negatives/positive and enhancing overall detection confidence. Notably, the proposed OPRCC-eLFS also exhibited comparable or even superior analytical performance than other reported CRISPR/Cas12a based methods on the basis of sensitivity, operational simplicity, and linear range (details in Table S2). Besides, considering the on-site screening application, this dual-mode OPRCC-eLFS could be miniatured as portable device for simultaneous colorimetric qualitative screening and electrochemical quantitative analysis, which holds greater superiority compared to common fluorescent assisted CRISPR/Cas12a methods.

In complicated food samples, multiple bacteria may often coexist, thus making selectivity a crucial criterion for evaluating the new proposed method. Consequently, the selectivity of the OPRCC-eLFS was assessed under identical detection conditions in the presence of other common bacteria, including *Cronobacter sakazakii* (*C. sakazakii*), *Staphylococcus aureus* (*S. aureus*), *Vibrio parahaemolyticus* (*V. parahaemolyticus*), *Pseudomonas aeruginosa* (*P. aeruginosa*), *Listeria monocytogenes* (*L. monocytogenes*), and *Escherichia coli* (*E. coli*). Control bacterial samples at concentrations of 10^6 CFU/mL and corresponding samples mixed with 10^4 CFU/mL *Salmonella* were measured with the OPRCC-eLFS. Additionally, the specificity of the OPRCC-eLFS was further evaluated using four different *Salmonella* serotypes (*Salmonella* ATCC 13076, CMCC 50093, CICC 10437, and CICC 21512), each tested at 10^4 CFU/mL. As shown in Fig. 4D, only *Salmonella* (regardless of serotype) or the mixed samples with the target *Salmonella* exhibited a significant reduction in the signal intensity on the T line of eLFS. The control pathogens, even at 100 times higher concentrations than for *Salmonella*, only displayed optical signals on the T line that are identical to that of the blank control. The corresponding electrochemical sensing results on the T line of eLFS show in Fig. 4E that only the target *Salmonella* induced distinguishable current variations, while the control bacteria did not, and, thus, indicating that the OPRCC-eLFS gave no response to the non-target bacteria. The primer set adopted in this research was designed to differentiate the strains of the bacteria and not precise to the serotypes of *Salmonella*, which effectively guarantee the specificity. And this excellent specificity of the OPRCC-eLFS is also ascribed to the presence of both RPA and CRISPR/Cas12a.

It is also very important that the proposed ORPCC-eLFS demonstrate very high reproducibility and stability for ensuring its effectiveness and reliability for practical applications. The repeatability was therefore evaluated by measuring the same *Salmonella* solution (3.84 × 10^4 CFU/

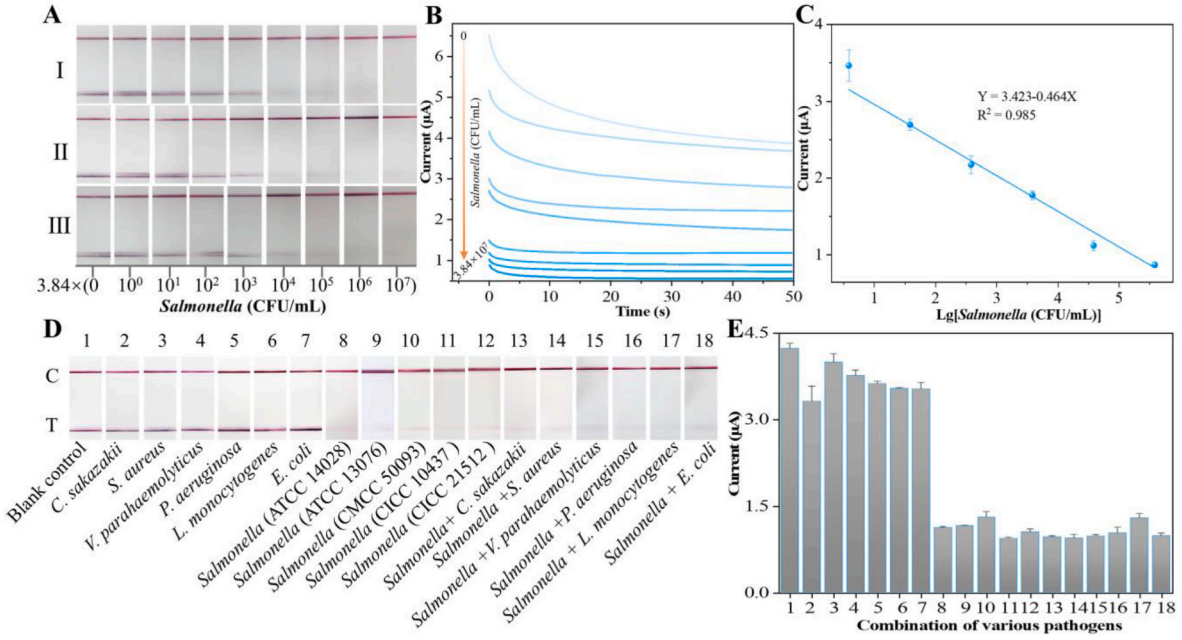


Fig. 4. (A) Visualization of *Salmonella* detection results at varying concentrations using the OPRCC-eLFS method. (B) Quantification of T-line signals for each eLFS from (A) using an electrochemical analysis method. (C) The linear relationship between T-line electrochemical signals and *Salmonella* concentrations. (D) Selectivity evaluation of OPRCC-eLFS detection of various pathogens and their mixtures. For combinations involving one or two pathogens, each non-target pathogen is kept at a concentration of 10^6 CFU/mL, while the target *Salmonella* concentration is fixed at 10^4 CFU/mL (the same for other serotypes of *Salmonella*). (E) Quantification of T-line electrochemical signals for each eLFS mentioned in (D).

mL) 10 times. A low variation of the ten measurements was subsequently confirmed with a relative standard deviation (RSD) of 6.42 % (Fig. S6A and B), indicating that the repeatability of the proposed OPRCC-eLFS is satisfactory. Additionally, the stability of the OPRCC-eLFS was validated by storing and reusing it for detection of *Salmonella* at 3.84 × 10^4 CFU/mL with three parallel measurements for varying durations (up to 30 days). Both the visual and chronoamperometric signals exhibited minimal fluctuation with RSD of 9.49 % of the current values after 30-day storage (Fig. S6C and D). Furthermore, batch-to-batch consistency was also investigated, yielding an acceptable RSD of 9.02 % of current values (Fig. S6E and F). These results demonstrate that the OPRCC-eLFS exhibited excellent stability and reproducibility for *Salmonella* detection.

3.5. Recovery of Salmonella in spiked samples

To assess the recovery efficiency of OPRCC-eLFS for *Salmonella* in real samples, four food samples with different matrix including milk, orange juice, eggs and salmon were spiked with *Salmonella* and then measured to determine the recovery efficiency. Within the spiked range (from 3.84 to 3.84 × 10^7 CFU/mL), the visual detection limit was achieved as 384 CFU/mL for all food matrices, while the electrochemical

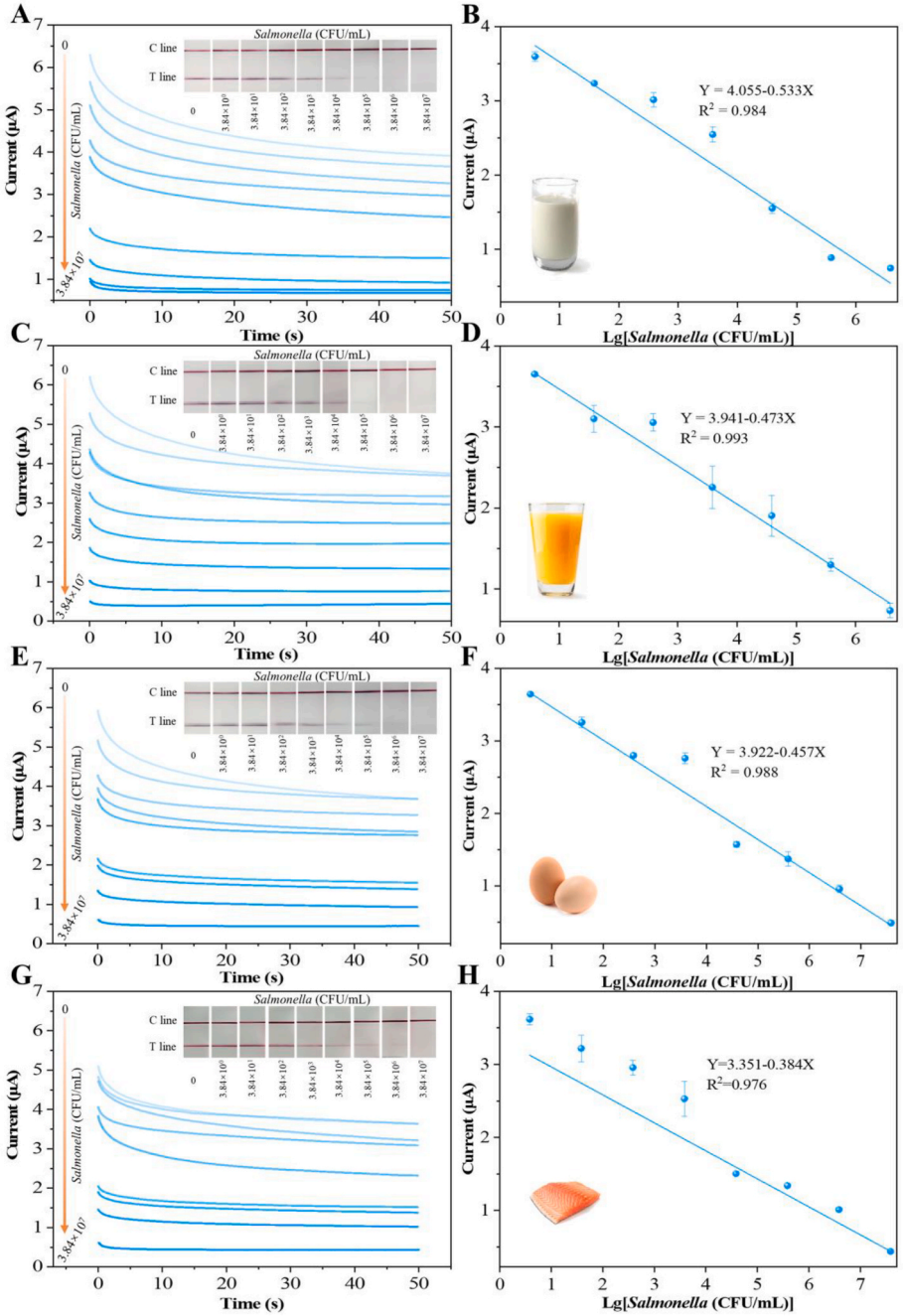


Fig. 5. Detection of *Salmonella* in real food samples: Milk samples: (A) OPRCC-eLFS dual-mode detection results, (B) linear equation correlating T-line electrochemical signals with *Salmonella* concentrations; Orange juice samples: (C) OPRCC-eLFS dual-mode detection results, (D) linear equation correlating T-line electrochemical signals with *Salmonella* concentrations; Egg samples: (E) OPRCC-eLFS dual-mode detection results, (F) linear equation correlating T-line electrochemical signals with *Salmonella* concentrations. Salmon samples: (G) OPRCC-eLFS dual-mode detection results, (H) linear equation correlating T-line electrochemical signals with *Salmonella* concentrations. (For interpretation of the references to color in this figure legend, the reader is referred to the Web version of this article.)

detection was achieved at 3.84 CFU/mL for milk samples and 38.4 CFU/mL for orange juice, egg and salmon samples (Fig. 5). These differences in detection limit and linearity among different samples may be attributed to the matrix effects of different food samples. Additionally, detection results with the commercial real time PCR kit (Fig. S7) were in well agreement with those of our method, confirming the accuracy and reliability of this developed dual-mode OPRCC-eLFS. The satisfactory sensitivity and specificity of OPRCC-eLFS for real samples is attributed to the double-recognition of RPA amplicons mediated CRISPR/Cas12a, along with the two-step signal amplification via redox reactions catalyzed by AuNPs on the T line of eLFS. Furthermore, the integration of visual and electrochemical detection modules effectively addresses detection requirements for different application scenarios.

4. Conclusion

We have successfully developed a novel and innovative dual-mode colorimetric and electrochemical detection platform, referred to as OPRCC-eLFS, for rapid, sensitive and reliable detection of *Salmonella* in different food samples. This platform integrates the simplicity of LFS-based qualitative colorimetric mode synergistically with the high sensitivity and quantitative capabilities of electrochemical mode, enabling simultaneous qualitative and quantitative detection of *Salmonella*. When applied to the detection of *Salmonella* in milk, juice, egg and salmon samples, this proposed dual-mode method outperformed previously reported two-step methods. Notably, this new developed OPRCC-eLFS effectively overcomes the intrinsic limitations of traditional methods, which often require use of multiple containers and multi-step procedures, by integrating RPA and CRISPR technologies into the one-pot reaction. This integration minimizes the risk of multiple reagent additions associated aerosol contamination. The dual-mode OPRCC-eLFS platform is user-friendly, time-efficient, and suitable for on-site applications. It provides an affordable solution for the rapid and continuous routine monitoring of *Salmonella* and other foodborne pathogens. Furthermore, the platform leverages the strengths of both techniques including the isothermal amplification, and cyclic cleavage, enhancing accuracy and sensitivity. Additionally, the inclusion of AuNPs serves as both the colorimetric signal tag for qualitative screening and the catalytic factor of the redox reactions used for quantitative electrochemical measurement, hence significantly improving the overall sensing performance of the OPRCC-eLFS. Meanwhile, the mutual calibration between the qualitative screening and quantitative analysis could further guarantee the accuracy of detection compared with single-mode methods. This proposed new dual-mode OPRCC-eLFS method further highlights and strengthen the use of molecular diagnostic technologies in food safety monitoring and biomedical diagnostics, thus contributing to advancements in these critical fields.

CRediT authorship contribution statement

Qi Chen: Writing – original draft, Methodology, Investigation. **Hang Wang:** Validation, Methodology. **Haoyang Xu:** Investigation. **Yubo Peng:** Methodology, Investigation. **Bangben Yao:** Validation. **Zhaoran Chen:** Validation. **Jiening Yang:** Validation. **Samuel Adeloju:** Writing – review & editing, Supervision. **Wei Chen:** Writing – review & editing, Writing – original draft, Supervision, Resources, Investigation, Funding acquisition.

Declaration of competing interest

The authors declare that they have no known competing financial interests or personal relationships that could have appeared to influence the work reported in this paper.

Acknowledgement

This work was supported by the grants received from the National Key Research Program (2024YFF0618104), the NSFC program (32172295), Shanghai S&T commission (22N31900500), the Hainan Key Research Program (ZDYF2022XDNY248), and the National Key Research Program (2023YFF0611500).

Appendix A. Supplementary data

Supplementary data to this article can be found online at https://doi.org/10.1016/j.bios.2025.117529.

Data availability

Data will be made available on request.

References

Ahamed, M.A., Khalid, M.A.U., Dong, M., Politza, A.J., Zhang, Z.K., Kshirsagar, A., Liu, T. Y., Guan, W.H., 2024. Biosens. Bioelectron. 246, 115866.
Chen, J.Y., Chen, Y., Huang, L.L., Lin, X.F., Chen, H., Xiang, W.W., Liu, L., 2024. Nat. Biotechnol. https://doi.org/10.1038/s41587-024-02255-7.
Cheng, X.K., Li, Y.R., Kou, J., Liao, D., Zhang, W.L., Yin, L.J., Man, S.L., Ma, L., 2022. Biosens. Bioelectron. 215, 114559.
Fu, X.R., Sun, J.D., Liang, R., Guo, H.Y., Wang, L.P., Sun, X.L., 2021. Trends Food Sci. Technol. 116, 115–129.
Galán, J.E., 2021. Nat. Rev. Microbiol. 19 (11), 716–725.
Gao, D., Ma, Z.Y., Jiang, Y.Y., 2022. Trac-Trend Anal Chem. 157, 116788.
Gu, K., Song, Z.X., Zhou, C.Y., Ma, P., Li, C., Lu, Q.Z., Liao, Z.W., Huang, Z.R., Tang, Y.Z., Li, H., Zhao, Y., Yan, W.J., Lei, C.W., Wang, H.N., 2022. J. Nanobiotechnol. 20 (1), 167.
Hu, T., Yu, Y.Y., Lin, Y., Chen, C.X., 2023. Anal. Chem. 95 (50), 18587–18594.
Jiang, H., Chang, W., Zhu, X.F., Liu, G., Liu, K.Y., Chen, W., Wang, H., Qin, P.Z., 2024. Anal. Chem. 96 (31), 12684–12691.
Lee, H., Yoon, Y., 2021. Food Sci Anim Resour 41 (1), 1–7.
Li, B., Wang, H.L., Xu, J.G., Qu, W., Yao, L., Yao, B.B., Yan, C., Chen, W., 2023. Food Sci. Hum. Wellness 12 (4), 1167–1173.
Li, H.Y., Peng, Y., Huang, X.D., Wan, R.Y., Zhang, L., Wang, X., Han, L.R., Li, L.S., Wang, C.F., Chen, J.L., 2024. Coord. Chem. Rev. 510, 215797.
Li, J.X., Khan, S., Gu, J., Filipe, C.D.M., Didar, T.F., Li, Y.F., 2023. Angew. Chem. Int. Ed. 62 (20), e202300828.
Lin, M., Yue, H., Tian, T., Xiong, E., Zhu, D., Jiang, Y., Zhou, X., 2022. Anal. Chem. 94 (23), 8277–8284.
Liu, Y.J., Singh, P., Mustapha, A., 2018. Food Control 91, 225–230.
Ma, L., Wang, J.J., Li, Y.R., Liao, D., Zhang, W.L., Han, X., Man, S.L., 2023. J. Hazard Mater. 443, 130234.
Mao, G.B., Luo, X., Ye, S.L., Wang, X., He, J., Kong, J.L., Dai, J.B., Yin, W., Ma, Y.X., 2023. Anal. Chem. 95 (20), 8063–8069.
Qiu, S., Liu, B., Leng, Y.K., Fox, E., Zhou, X., Yan, B.B., Sang, X.Z., Long, K.P., Fu, Y.J., He, X.D., Yuan, J.H., Farrell, G., Wu, Q., 2023. Biosens. Bioelectron. 234, 115337.
Ren, Y.R., Wei, J., Wang, Y., Wang, P., Ji, Y.W., Liu, B.Y., Wang, J.L., González-Sapienza, G., Wang, Y.R., 2022. Anal. Chim. Acta 1203, 339705.
Shen, Y.F., Jia, F., He, Y.W., Fu, Y.C., Fang, W.H., Wang, J.P., Li, Y.B., 2022. Biosens. Bioelectron. 213, 114437.
Shen, Y.F., Xu, L.Z., Li, Y.B., 2021. Compr Rev Food Sci F. 20 (1), 149–197.
Song, J., Cha, B., Moon, J., Jang, H., Kim, S., Jang, J., Yong, D., Kwon, H.J., Lee, I.C., Lim, E.K., Jung, J., Park, H.G., Kang, T., 2022. ACS Nano 16, 11300–11314.
Tan, Q., Shi, Y., Duan, C., Li, Q., Gong, T., Li, S., Duan, X., Xie, H., Li, Y., Chen, L., 2024. J. Med. Virol. 96 (4), 29624.
Vieira, K.C.D., da Silva, H.R.A., Rocha, I.P.M., Barboza, E., Eller, L.K.W., 2022. Crit Rev. Food Sci. 62 (24), 6726–6741.
Wang, P., Guo, B., Zhang, X., Wang, Y., Yang, G., Shen, H., Gao, S., Zhang, L.H., 2023. J. Agric. Food Chem. 71 (16), 6490–6498.
Wang, X.Y., Yang, T., Zhang, Y.L., Zeng, Z.Y., Wei, Q., Chen, P., Yang, S.S., Huang, Y.F., Zhang, Y.Q., Lu, H.L., Wu, L.H., Tang, D.J., Yang, P., Wang, X.C., Liu, Q., Li, F., Ling, C., Huang, S.F., 2024. Anal. Chem. 96 (44), 17567–17575.
Wang, Z.X., Zhao, J., Xu, X.X., Guo, L.L., Xu, L.G., Sun, M.Z., Hu, S.D., Kuang, H., Xu, C. L., Li, A.K., 2022. Small Methods 6 (1), 2101143.
Wei, X.Y., Zhao, X.H., 2021. Curr opin. Food Sci. (N. Y.) 37, 52–57.
Wu, X.L., Lou, X.M., Zhou, H.Z., Raymond, J.J., Kwang, L.G., Ong, F.Y.T., Springs, S.L., Yu, H., 2024. Trends Food Sci. Technol. 145, 104349.
Yang, L., Chen, G.W., Wu, J., Wei, W., Peng, C., Ding, L., Chen, X.Y., Xu, X.L., Wang, X.F., Xu, J.F., 2024. Anal. Chem. 96 (14), 5471–5477.
Yin, X.Y., Yang, L.L., Sun, X.Y., Zheng, Q.Y., Piao, Y.Z., Hu, B., Zhang, X.B., Cao, J.J., 2024. Food Chem. 438, 137952.

Younes, N., Yassine, H.M., Kourentzi, K., Tang, P.T., Litvinov, D., Willson, R.C., Abu-Raddad, L.J., Nasrallah, G.K., 2024. Crit Rev. Food Sci. 64 (27), 9910–9932.
Zhang, L.F., Luo, S.H., Li, W.B., Su, W.T., Chen, S.T., Liu, C.C., Pan, W.L., Situ, B., Zheng, L., Li, L., Yan, X.H., Zhang, Y., 2024. J. Nanobiotechnol. 22 (1), 602.
Zhong, Y., Ling, L., Wang, J.L., Wang, W., Zhang, X.B., Hu, B., Chen, W.R., Zheng, Q.Y., Cao, J.J., 2025. Food Control 168, 110949.